Review of Scientific Instruments

In situ calibration of neutron activation system on the large helical device

Cite as: Rev. Sci. Instrum. **88**, 113302 (2017); https://doi.org/10.1063/1.5009475
Submitted: 26 April 2017 • Accepted: 15 October 2017 • Published Online: 06 November 2017

N. Pu, T. Nishitani, M. Isobe, et al.

In situ calibration of neutron activation system on the large helical device

N. Pu,[1] T. Nishitani,[2] M. Isobe,[1,2] K. Ogawa,[1,2] H. Kawase,[1] T. Tanaka,[3] S. Y. Li,[3] S. Yoshihashi,[3] and A. Uritani[3]
[1]*SOKENDAI (The Graduate University for Advanced Studies), 322-6 Oroshi-cho, Toki 509-5292, Japan*
[2]*National Institute for Fusion Science, National Institutes of Natural Sciences, 322-6 Oroshi-cho, Toki 509-5292, Japan*
[3]*Nagoya University, Furo-cho, Nagoya 464-8603, Japan*

(Received 26 April 2017; accepted 15 October 2017; published online 6 November 2017)

In situ calibration of the neutron activation system on the Large Helical Device (LHD) was performed by using an intense ^{252}Cf neutron source. To simulate a ring-shaped neutron source, we installed a railway inside the LHD vacuum vessel and made a train loaded with the ^{252}Cf source run along a typical magnetic axis position. Three activation capsules loaded with thirty pieces of indium foils stacked with total mass of approximately 18 g were prepared. Each capsule was irradiated over 15 h while the train was circulating. The activation response coefficient $(9.4 \pm 1.2) \times 10^{-8}$ of ^{115}In(n, n′)^{115m}In reaction obtained from the experiment is in good agreement with results from three-dimensional neutron transport calculations using the Monte Carlo neutron transport simulation code 6. The activation response coefficients of 2.45 MeV birth neutron and secondary 14.1 MeV neutron from deuterium plasma were evaluated from the activation response coefficient obtained in this calibration experiment with results from three-dimensional neutron calculations using the Monte Carlo neutron transport simulation code 6. *Published by AIP Publishing.* https://doi.org/10.1063/1.5009475

I. INTRODUCTION

The Large Helical Device (LHD) is a large superconducting heliotron device in Japan, having a major radius of 3.9 m and averaged plasma minor radius of ~0.6 m.[1] In the LHD, the deuterium plasma operation was conducted from March 2017 to explore further high-performance deuterium plasmas. Neutron yield measurement is essential for the LHD deuterium project in terms of radiation safety, the evaluation of fusion output, and the study of energetic-particle confinement. To evaluate the total neutron yield from LHD deuterium plasmas, a wide dynamic range neutron flux monitor (NFM)[2] and a neutron activation system (NAS) are employed in the LHD.[3] The NFM in the LHD consists of three ^{235}U fission chambers and three highly sensitive thermal neutron detectors. The NFM plays the primary role in evaluating the total neutron yield. Although the NAS does not provide time evolution of the neutron emission rate, it is completely insensitive to the gamma ray and is of great value for performing cross check of the neutron yield evaluated by the NFM.[4,5] The triton burnup study is one of the important physics subjects in the LHD deuterium project to demonstrate alpha particle confinement in the LHD-type magnetic field configuration. The NAS also performs an important role in the triton burnup study through measurements of the secondary 14.1 MeV neutron yield.

In tokamaks such as TFTR,[6] JET,[7] ASDEX-U,[8] and JT-60U,[9] neutron activation techniques have been applied to measure the neutron yield from deuterium plasmas. The activation response coefficients of NASs were evaluated from the results of the Monte Carlo neutron transport simulation code (MCNP)[10] in those devices. Limited points of *in situ* calibration experiments for NASs were performed in TFTR,[11] JET,[12] and FTU[13] by using neutron sources, but not by toroidal shape sources. The machine structure of the LHD is extremely complicated in comparison with tokamaks, and the activation response coefficients of the NAS should be obtained from the experiment in addition to the simulation. The LHD has enough space to install a railway, support structures, and a train loaded with the neutron source running along the magnetic axis position inside the vacuum vessel to simulate a ring-shaped neutron source. In November 2016, the *in situ* absolute calibration of the NFM and NAS was carried out in the LHD by using an approximately 800 MBq ^{252}Cf neutron source. This *in situ* calibration of the NAS was performed for the first time in the world on a fusion device.

In this paper, the introduction of NAS on the LHD, the calibration neutron source, and the detection efficiencies of the high-purity germanium (HPGe) detector are described in Sec. II. The principle of measurement is described in Sec. III. The *in situ* calibration experiment is shown in Sec. IV. Activation response coefficients of the NAS for 2.45 MeV neutrons and secondary 14.1 MeV neutrons from real deuterium plasma were calculated by the MCNP code. Those results based on the MCNP simulation are discussed in Sec. V. Finally, the conclusions are given in Sec. VI.

II. EXPERIMENTAL SETUP

A. Neutron activation system on the LHD

The NAS on the LHD is a so-called rabbit system, consisting of the activation foils, the capsule, pneumatic control systems, two irradiation ends, pneumatic tubes, air compressor, launching/collecting station, and two HPGe gamma-ray detectors as shown in Fig. 1. The system design of the NAS is based on that used in JT-60U.[9] The activation foil is mounted

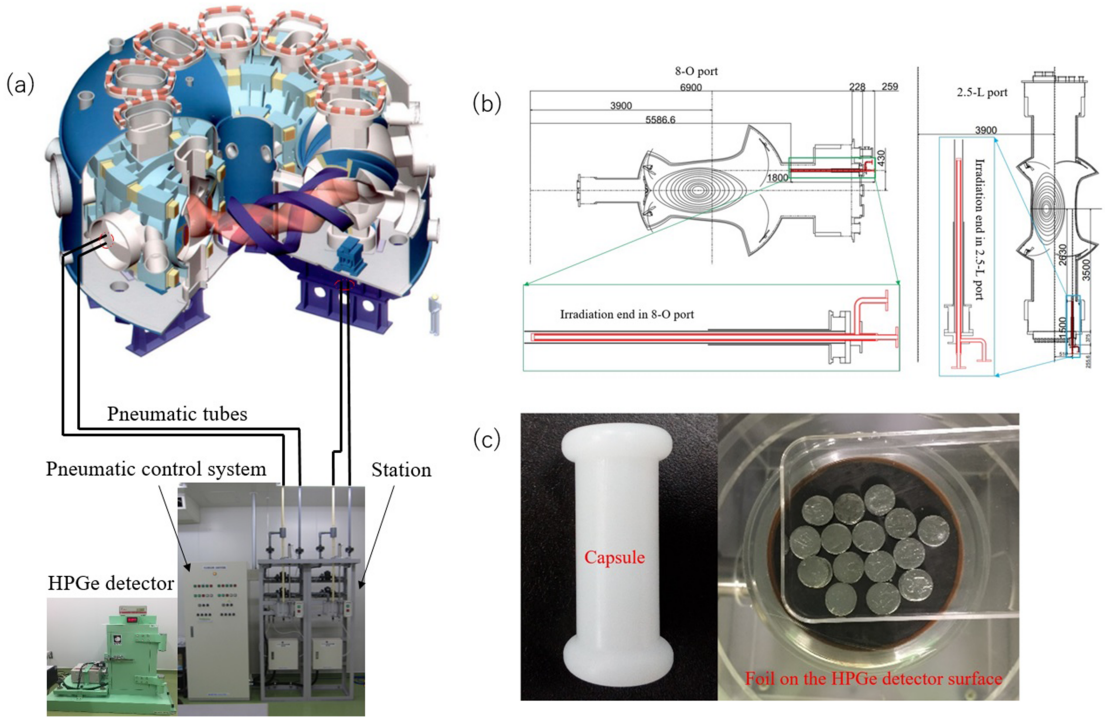

FIG. 1. (a) Overview of neutron activation system on the LHD, (b) two irradiation ends of neutron activation system at two poloidal cross sections of 8-O and 2.5-L ports, (c) the left photograph is of the capsule, and the right photograph is of the indium foil pieces on the surface of the HPGe detector.

on a capsule made of polyethylene. The capsule loaded with the activation foils is transferred through a pneumatic tube from the station to the irradiation end. There are two irradiation ends: one is at the 8-O horizontal port, which is located at the outboard side of the horizontally elongated poloidal cross section of the plasma, and the other is located at the 2.5-L lower port, which is under the vertically elongated cross section of the plasma as shown in Fig. 1(b). Each irradiation end is made of stainless steel with a coaxial structure. Outside the port flange, the inner tube of the irradiation end is connected to a capsule transfer tube made of acrylonitrile-butadiene-styrene resin and the outer tube is connected to a vinyl chloride resin tube for compressed air supply and exhaust. The length of the pneumatic tubes in the 8-O port line and the 2.5-L port line is 93 m and 80 m, respectively.

During the LHD experiment, the capsule will be transferred to the irradiation end before discharge initiation by receiving a trigger pulse before the discharge. After the discharge, the capsule will be transferred to the station for the measurement of gamma-ray spectroscopy within the specified time. In the automatic control mode, this specified time can be set in the pneumatic control system by hand according to the discharge duration. In the manual control mode, a capsule can be launched and transferred back at any time. The transfer time from the irradiation end to the station is about 20 s, which depends on the pressure of compressed air. Each tube has a manometer to monitor the air pressure.

The HPGe detector is essentially required to identify nuclides of our interest through gamma-ray spectroscopy with high energy resolution. The HPGe detector used in this work is manufactured by Canberra Industries, Inc. (Model: GX3018/CP5-PLUS-U). The detector has a very thin window made of carbon composites on the front surface, which reduces the gamma-ray shielding effect of the window and extends the useful energy range down to 3 keV. The effective diameter and thickness of the germanium crystal of the HPGe detectors are 61.80 mm and 39.80 mm, respectively. The distance from the window to the surface of the HPGe detectors is 5.00 mm. Because the detector is in a lead shield having the thickness of 100 mm, the background pulse counting rate due to external sources is low enough for our purpose. Output pulses from the preamplifier are fed into the multichannel analyzer, the DSA-LX produced by Canberra Industries, Inc., based on advanced digital signal processing techniques, and data are analyzed on a personal computer.

The foil size is 10 mm in diameter and 1 mm in thickness. The indium foil is employed for the 2.45 MeV measurements by utilizing ^{115}In(n, n′)^{115m}In reaction, because the reaction has a threshold of 336 keV, a half-life of 4.486 h, and a rather large cross section. For the secondary 14.1 MeV neutron yield measurement, silicon foil and aluminum foil are used with ^{28}Si(n, p)^{28}Al, ^{27}Al(n, p)^{27}Mg, and ^{27}Al(n, α)^{24}Na reactions. The triton burnup ratio can be evaluated by the measurements of indium, silicon, and aluminum. In this calibration experiment, a foil stack with thirty pieces of indium foils, as shown in Fig. 1(c), is used to obtain the sufficient statistical error for a much weaker neutron yield compared with that in real plasmas.

B. Calibration neutron source

To simulate the toroidal plasma neutron source, the ring-shaped source must be created. Figure 2(a) shows the source

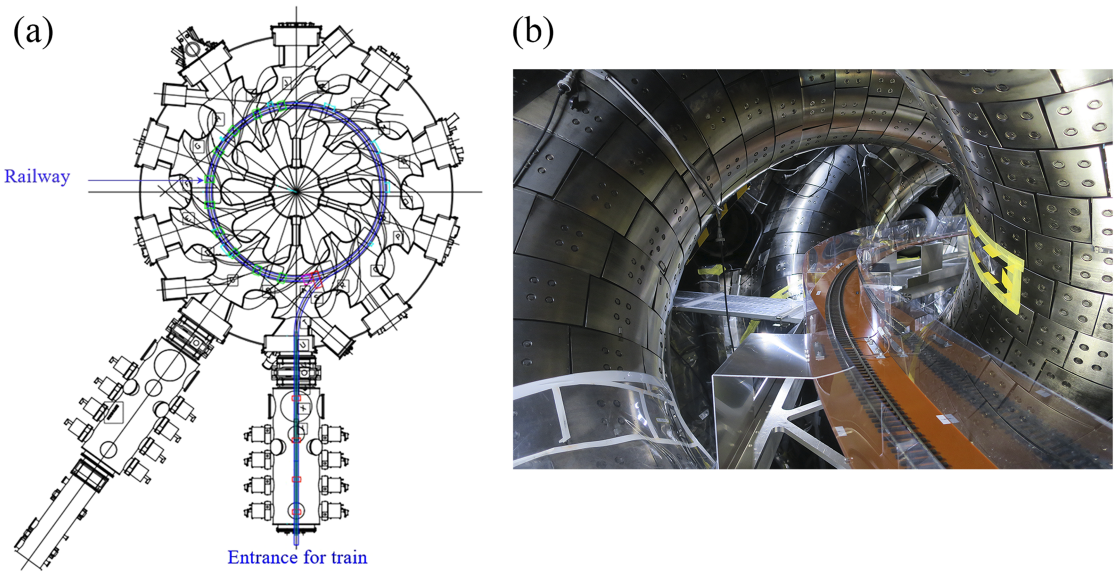

FIG. 2. (a) Horizontal layout diagram of *in situ* calibration experiment by using ^{252}Cf neutron source; (b) the photograph of the railway inside the LHD vacuum vessel.

transport system by using a toy train rail with 36 mm rail width, the so-called O-gauge rail. The train is loaded with a neutron source to circulate on the magnetic axis position at the major radius of 3.744 m inside the LHD vacuum chamber for generating a ring-shaped neutron source. The rail is fixed on the Bakelite plate which is installed on the maintenance stage made of aluminum frames as shown in Fig. 2(b).

An approximately 800 MBq ^{252}Cf neutron source by spontaneous fission was chosen for the *in situ* calibration because the mean neutron energy of neutrons emitted from ^{252}Cf is approximately 2.1 MeV, which is close to that of neutrons produced by D–D reaction. The ^{252}Cf neutron source releases 3.7 neutrons on average per spontaneous fission event, which is almost 3.1% of the decay. The half-life is approximately 2.646 years. The precise birth neutron emission rate was $(1.34 \pm 0.014) \times 10^8$ n/s at 12:00 GMT on April 27, 2015, which was calibrated at National Physics Laboratory, United Kingdom. Therefore, the birth neutron emission rate is 8.93×10^7 n/s on November 9, 2016.

C. Efficiencies of the HPGe detector

Before the *in situ* calibration, the detection efficiencies of the HPGe detector were calibrated by using the standard gamma-ray sources placed on the surface of the HPGe detector. The standard sources are the volumetric gamma-ray sources made by mixed powder gamma-ray sources of different types of nuclides in the U-8 container. The detection efficiencies obtained by using the standard sources are shown in Fig. 3. In the *in situ* calibration experiment, thirty pieces of activated foils ware placed on the surface of the HPGe detector. The geometry of the standard gamma-ray sources and the activated foil source are significantly different. Therefore, the efficiencies of the HPGe detector for 336 keV (^{115m}In), 843 keV (^{27}Mg), 1368 keV (^{24}Na), and 1779 keV (^{28}Al) gamma rays of the activated foils were evaluated with the assistance of the simulation calculation using the Particle and Heavy Ion Transport code System (PHITS)[14] as shown in Fig. 3. The thirty pieces of foil stack was uniformly distributed on the surface of the HPGe detector in the model of the PHITS code. At first, we calculated efficiencies of the thirty pieces of indium foil, silicon foil, and aluminum foil without the self-absorbed effect, which is the absorption of gamma rays by the foil material itself, where the foil density is assumed to be the same as the air density. Next, we calculated detection

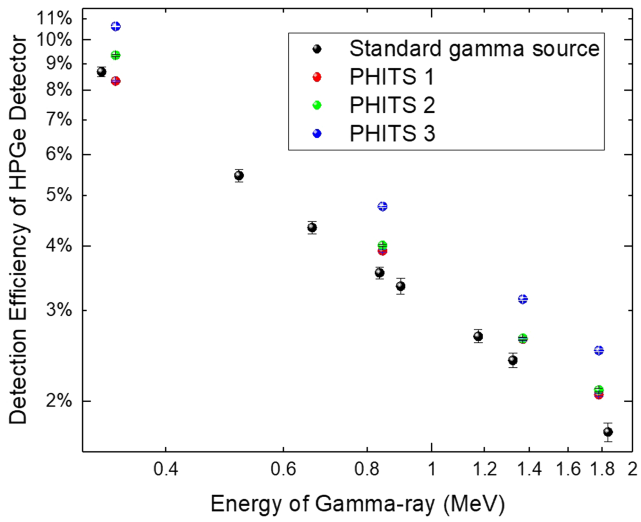

FIG. 3. Detection efficiencies of the HPGe detector. Red, blue, and green dots stand for the efficiencies of the HPGe detector for 336 keV (^{115m}In), 843 keV (^{27}Mg), 1368 keV (^{24}Na), and 1779 keV (^{28}Al) gamma-rays of the activated foils calculated by the PHITS code. "PHITS 1" represents calculation results of the case of thirty pieces of foil with self-absorbed effect. "PHITS 2" stands for the calculation results of the case of thirty pieces of foil without self-absorbed effect. "PHITS 3" is the calculation results for the case of one piece of foil with self-absorbed effect. Black dots stand for the detection efficiencies of the HPGe detector calibrated by the volume standard gamma-ray source.

efficiencies of thirty pieces of indium foil, silicon foil, and aluminum foil with the self-absorbed effect by using the actual density of the foil, where self-absorbed effect on the detection efficiency is clearly observed. In the results of the model with the self-absorbed effect, the self-absorbed effect of thirty pieces of indium foils for 336 keV is larger than the self-absorbed effect of thirty pieces of silicon foils and aluminum foils for high-energy gamma rays. Thus, we used the detection efficiency with the self-absorbed effect. In addition, the efficiencies of one piece of indium foil, silicon foil, and aluminum foil on the center of the surface of the HPGe detector with self-absorbed effect also were evaluated by the PHITS code for plasma experiments. In the one piece case model, the actual sizes of the HPGe detector and foil were also considered.

III. PRINCIPLE OF MEASUREMENT

The averaged neutron emission rate S_n [s^{-1}] can be calculated by the expression

$$S_n = \frac{\lambda \cdot C}{N \cdot \alpha_\gamma \cdot \varepsilon \cdot (e^{-\lambda t_1} - e^{-\lambda t_2}) \cdot (1 - e^{-\lambda t_0}) \cdot \sum_E \sigma(E) \cdot \Phi(E)}.$$

In addition, the total neutron yield can be obtained as

$$Y_n = S_n \cdot t_0.$$

Here, the activation response coefficients can be defined as reaction rate for unit source neutron and unit sample nuclei number. Thus the activation response coefficients of the NAS per unit source neutron and unit target nuclei can be expressed as follows:

$$\sum_E \sigma(E) \cdot \Phi(E) = \frac{\lambda \cdot C}{N \cdot S_n \cdot \alpha_\gamma \cdot \varepsilon \cdot (e^{-\lambda t_1} - e^{-\lambda t_2}) \cdot (1 - e^{-\lambda t_0})}.$$

In those expressions, $\sigma(E)$ is the cross section of the reaction [b], $\Phi(E)$ is neutron spectrum in the irradiation end for unit source neutron [$cm^{-2} \cdot s^{-1}$], E is the neutron energy, $N = \alpha_{is} \cdot m \cdot N_A / M$ is the number of sample nuclei, α_{is} is the isotopic fraction of the sample nuclide, m is the mass of the sample [g], N_A is the Avogadro's constant [mol^{-1}], M is the molar mass of the nuclide [g/mol], α_γ is the gamma ray abundance, t_0 is the end of irradiation time [s], t_1 is the start time of the gamma-ray measurement from the start of the irradiation [s], t_2 is the end time of the gamma-ray measurement from the start of the irradiation [s], λ is the decay constant of activated nuclide in the sample, C is the gamma-ray count under the specific gamma-ray peak measured during t_1 to t_2, and ε is the efficiency of the HPGe detector in the specific gamma-ray peak.[15]

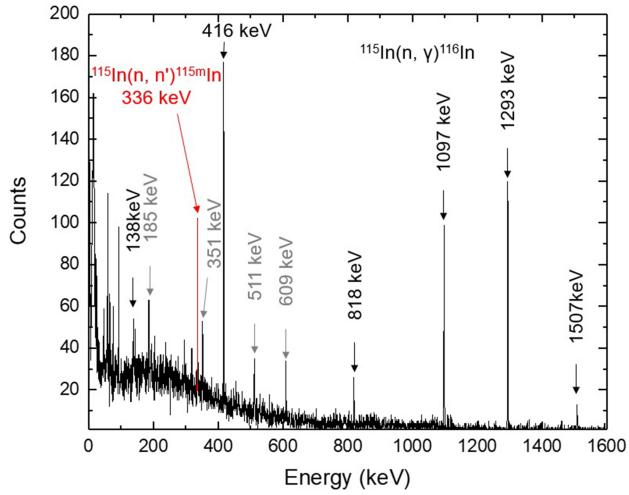

FIG. 4. The gamma-ray spectrum for thirty pieces of indium foils was obtained from 10 000 s measurement by the HPGe detector. Here, red font stands for ^{115}In(n, n')^{115m}In reaction, black font stands for ^{115}In(n, γ)^{116}In reactions, and gray font is not a gamma ray from indium.

IV. EXPERIMENTAL RESULTS

In the *in situ* calibration experiment, three capsules were irradiated over 15 h at the 8-O port. Each capsule has thirty pieces of indium foils inside and the total mass of indium is approximately 18 g. The capsule cannot be transferred by using the NAS pneumatic tube due to insufficient air pressure. The neutron flux of irradiation end in the 2.5-L port is lower

TABLE I. Activation response coefficients (ARC) of the ^{252}Cf ring-shaped neutron source.

	Capsule #1			Capsule #2			Capsule #3		
Mass (g)	17.785			17.717			17.678		
Irradiation time (h)	15.217			15.583			46.283		
Run number	Counting time (s)	Counts	ARC	Counting time (s)	Counts	ARC	Counting time (s)	Counts	ARC
1st	3 000	29.8[a]	9.2×10^{-8}	3 000	85.6	1.1×10^{-7}	3 000	71.1	8.5×10^{-8}
2nd	3 000	56[a]	8.8×10^{-8}	10 000	164.9	8.7×10^{-8}	3 000	63.7	8.7×10^{-8}
3rd	10 000	162	9.8×10^{-8}	10 000	85	7.1×10^{-8}	10 000	171.2	9.2×10^{-8}
4th	10 000	111	1.0×10^{-7}	3 000	22.375	8.3×10^{-8}	10 000	121	1.1×10^{-7}
5th							10 000	64.5	9.1×10^{-8}
6th							40 000	115	1.1×10^{-7}

[a]Note that in the run number 1 measurement for the capsule #1, the gamma-ray was measured for thirty pieces of indium foils with the capsule. In the run number 2 measurement for the capsule #2, the gamma-ray was measured for twenty-nine pieces of indium foils without the capsule. In the other measurements, gamma-ray measurements were performed for the thirty pieces of indium foils without the capsule.

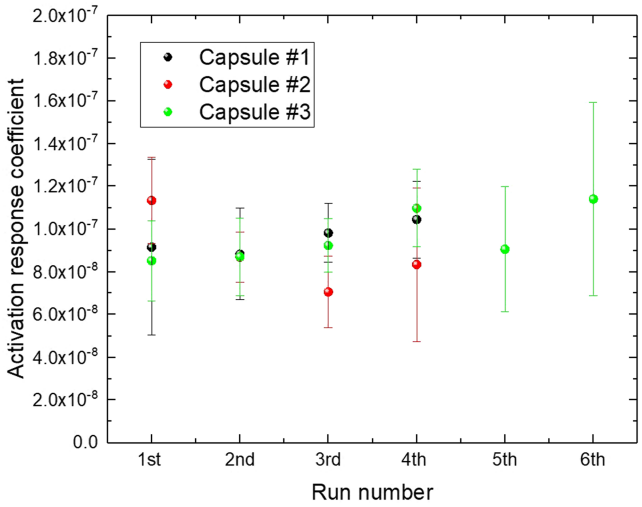

FIG. 5. Activation response coefficients of the ^{252}Cf ring-shaped neutron source for run number of each capsule were obtained from the *in situ* calibration experiment.

than that in the 8-O port because the irradiation end in the 2.5-L port is far from the plasma compared with the distance from the irradiation end in the 8-O port to the plasma. In addition to this, it is not easy to support the capsule inside the irradiation end in the 2.5-L port. Therefore, the capsule was placed inside the 8-O port and removed by hand. Immediately after the irradiation, the capsule was removed for gamma-ray measurement. The irradiation times of capsule #1, capsule #2, and capsule #3 are 15.217 h, 15.583 h, and 46.283 h, respectively. Multiple measurements were performed to improve the statistical error and to eliminate the effect of the gamma rays from ^{115}In(n, γ)^{116}In reactions. Each measurement time of the gamma rays ranged from 3000 s to 10 000 s in order to ensure that there are sufficient statistics of the photoelectric peak counts for the gamma ray of interest. The integrated photoelectric peak pulse counts of 336 keV gamma ray are evaluated by Gaussian fitting as shown in Fig. 4. The thirty pieces of irradiated indium foils were uniformly distributed on the surface of the HPGe detector and were measured simultaneously. The detection efficiencies of the HPGe detector for thirty pieces of indium foil measurement are evaluated by the PHITS code.

In Table I, the activation response coefficients obtained by multiple gamma-ray measurements of each capsule are listed and those are plotted for each run number in Fig. 5. The standard deviation of each counting is 13%. The error of the detection efficiencies of the HPGe detector from the PHITS calculation is 0.98%. Also, there is an error in irradiation time because it took approximately 2 min to place the capsule and to remove the capsule at the irradiation end. This error is considered to be 0.22% for total irradiation time of each capsule. The error of ^{252}Cf neutron source neutron emission rate is 1%. The total error of the calibration experiment is estimated to be approximately 13%. Thus the mean activation response coefficients of ^{115}In(n, n′)^{115m}In reaction is evaluated to be $(9.4 \pm 1.2) \times 10^{-8}$.

V. DISCUSSION BASED ON MCNP SIMULATION

The neutron spectrum Φ(E) in the irradiation end normalized for the unit source neutron is obtained from MCNP simulation. Activation response coefficients $\sum\sigma(E)\cdot\Phi(E)$ also can be obtained from MCNP simulation. Here, MCNP6 code[10] and nuclear data library FENDL 3.0[16] are used for the Φ(E) calculation, and JENDL 99 Dosimetry file[17] is used for the reactivity calculation. The rotation time, about 40 s, of the calibration neutron source on the magnetic axis is sufficiently shorter than the half-life of ^{115m}In. Therefore, this source can be regarded as a toroidal ring-shaped source by averaging a long-time effect. Actually, the neutron source in the plasma has poloidal distribution. The ^{252}Cf neutron source is a point source and is nearly isotropic in neutron emission. The model for the ^{252}Cf ring-shaped source is shown in Fig. 6(a), where detailed components are considered carefully, such as the irradiation end [enlarged part of Fig. 6(b)], the train, the railway, the maintenance support, and the model of superconducting coils without liquid helium. In the ^{252}Cf ring-shaped source case, the source neutron energy has a fission neutron spectrum represented by the Watt formula[10] $\frac{dN}{dE} \propto e^{(-E/a)} \cdot \sinh(bE)^{1/2}$, where $a = 1.18$ and $b = 1.034\,19$. Meanwhile, the foil stack of thirty pieces inside the capsule is modeled to estimate the

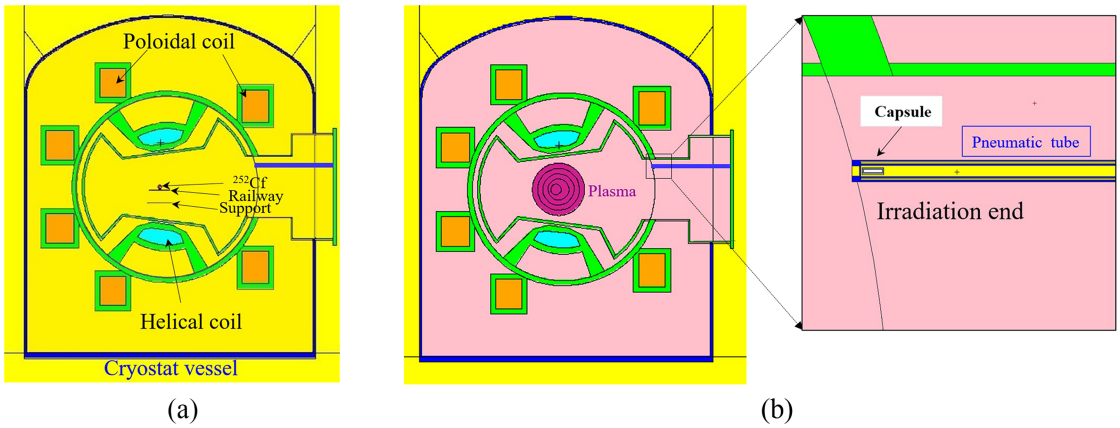

FIG. 6. (a) MCNP model for ^{252}Cf source; (b) MCNP model for plasma source and enlarged irradiation end.

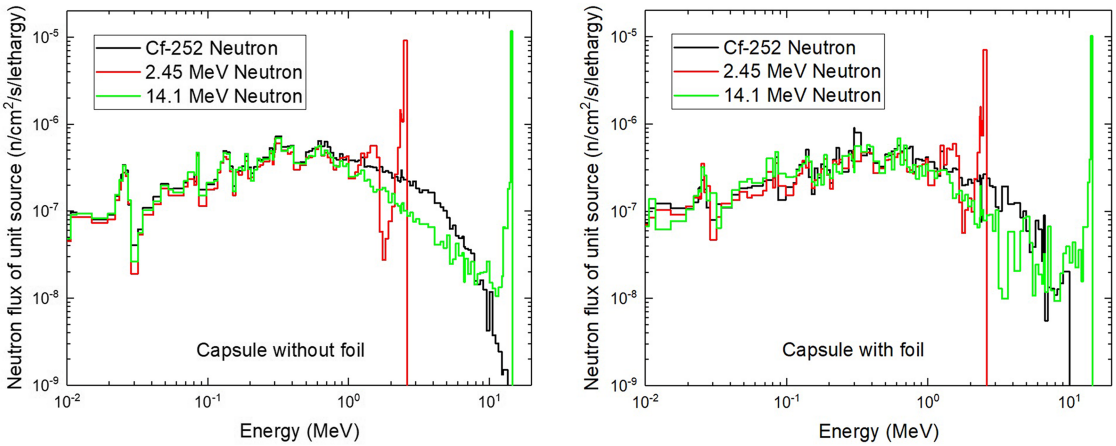

FIG. 7. (a) The neutron spectra normalized by unit source in the capsule without the foil in the ^{252}Cf neutron case and two plasma source cases; (b) the neutron spectra normalized by unit source in the capsule with thirty pieces of indium foils in the ^{252}Cf neutron case and one piece of foil in two plasma source cases.

self-shielding effect of the foil stack. The activation response coefficients of ^{115}In(n, n′)^{115m}In reaction for the ^{252}Cf ring-shaped source case was evaluated to be 8.8×10^{-8} (statistical error 4.2%) by the MCNP calculation. It is in good agreement with the result of the calibration experiment within 7% difference. This indicates that the MCNP calculation taking account of the self-shielding effect of the foil stack is sufficiently accurate.

In order to obtain the activation response coefficients for the plasma source, differences between the plasma source and the ^{252}Cf ring-shaped source have been evaluated by the MCNP. In the model for the plasma, the neutron source is a volumetrically monoenergetic neutron with a neutron emission density profile which is the structure of five coaxial torus geometry, as shown in Fig. 6(b). The neutron emission probability of five coaxial torus regions is determined to fit the typical neutron emission profile estimated in the LHD deuterium plasma. Meanwhile, only one piece of activation foil is modeled to simulate the measurement at the plasma experiment. The model of superconducting coils has liquid helium. Other main structures of the LHD are the same. The neutron spectra normalized by the unit source in the capsule without and with foil for the neutron from ^{252}Cf neutron, 2.45 MeV neutron, and 14.1 MeV neutron are shown in Figs. 7(a) and 7(b), respectively. In the incoming neutron spectra for the capsule without foil case shown in Fig. 7(a), there are significant differences in three spectra above 1 MeV. The ^{252}Cf fission neutron spectrum has high-energy component, while the neutron is mono-energetic in the plasma case. The low energy parts of the spectra are almost the same. This means that scattered neutrons from the LHD models for the ^{252}Cf ring-shaped source and plasma of volume neutron emission are almost the same. By comparing with Figs. 7(a) and 7(b), there are several differences in the neutron spectra of ^{252}Cf neutron, 2.45 MeV neutron, and 14.1 MeV neutron for the capsules without and with foil cases, respectively. Here, thirty pieces of the indium foil inside the capsule were modeled in the MCNP calculation for the ^{252}Cf ring-shaped source in the case of capsule with foil. Meanwhile, one piece of indium foil, silicon foil, and aluminum foil in the capsule was modeled for 2.45 MeV and 14.1 MeV plasma neutron source in the case of capsule with foil. In the case of capsule without a foil, there is only air in the capsule. Thus, the self-shielding effect of the foil for neutron was calculated by the MCNP in the case of capsule with foil. Those reasons would lead to the differences in the activation response coefficients for each reaction in the ^{252}Cf ring-shaped source case and the plasma case.

We consider that the difference of 7% between the *in situ* calibration and the MCNP calculation in the ^{252}Cf ring-shaped source case is mainly due to the modeling error in the MCNP calculation. Therefore, 7% is assumed to be a modeling error in the MCNP calculation not only for ^{115}In(n, n′)^{115m}In reaction but also for other reactions in plasma case to be used in the NAS measurement on the LHD. Here, we assumed that the error from cross section is less than 5%. By using those errors and the statistical error from the MCNP calculation for other

TABLE II. Activation response coefficients for plasma case calculated by the MCNP code for all reactions.

Reaction (neutron source)	Activation response coefficients	MCNP statistical errors (%)	Total error (%)
^{115}In(n, n′)^{115m}In (2.45 MeV neutron)	1.5×10^{-7}	3.4	9.3
^{28}Si(n, p)^{28}Al (14.1 MeV neutron)	8.4×10^{-8}	5.7	10
^{27}Al(n, p)^{27}Mg (14.1 MeV neutron)	2.4×10^{-8}	5.6	10
^{27}Al(n, α)^{24}Na (14.1 MeV neutron)	3.6×10^{-8}	5.8	10

reactions, we can evaluate the total error for each reaction in the plasma case. The activation response coefficients for the 2.45 MeV neutron from the D–D plasma case and for the secondary 14.1 MeV neutron are evaluated by using the MCNP calculation in Table II.

VI. CONCLUSION

The activation response coefficients were obtained for the ^{252}Cf neutron source by using detection efficiency of the HPGe detector, which was evaluated by the PHITS code. The activation response coefficients were in good agreement with the MCNP result. The activation response coefficients for the 2.45 MeV neutron from the D–D plasma and secondary 14.1 MeV neutron were evaluated by the assistance of the MCNP 6 calculation. The difference of 7% from in situ calibration and MCNP calculation for ^{252}Cf neutron case was utilized to estimate the error from MCNP model for the plasma case. This *in situ* calibration will be a good reference for future calibration experiments of fusion devices such as ITER.

ACKNOWLEDGMENTS

The authors would like to thank the LHD Experiment Group for their great contributions of the *in situ* calibration work for the neutron flux monitor and the neutron activation system. In addition, we would like to thank Dr. Guoqiang Zhong, Dr. Liqun Hu, Dr. Yuri Kashchuk, Dr. Vitaly Krasilnikov, Dr. Mamiko Sasao, Dr. Tieshuang Fan, and Dr. Mr. Lijian Ge for fruitful discussion in this work. This work was supported by the LHD project budgets (Nos. ULGG801, ULHH003, and ULHH034). This work was partly performed with the support and under the auspices of the NIFS Collaboration Research Program (No. KOAH033).

[1]A. Iiyoshi, A. Komori, A. Ejiri, M. Emoto, H. Funaba, M. Goto, K. Ida, H. Idei, S. Inagaki, S. Kado, O. Kaneko, K. Kawahata, T. Kobuchi, S. Kubo, R. Kumazawa, S. Masuzaki, T. Minami, J. Miyazawa, T. Morisaki, S. Morita, S. Murakami, S. Muto, T. Mutoh, Y. Nagayama, Y. Nakamura, H. Nakanishi, K. Narihara, K. Nishimura, N. Noda, S. Ohdachi, N. Ohyabu, Y. Oka, M. Osakabe, T. Ozaki, B. J. Peterson, A. Sagara, S. Sakakibara, R. Sakamoto, H. Sasao, M. Sasao, K. Sato, M. Sato, T. Seki, T. Shimozuma, M. Shoji, H. Suzuki, Y. Takeiri, K. Tanaka, K. Toi, T. Tokuzawa, K. Tsumori, K. Tsuzuki, K. Y. Watanabe, T. Watari, H. Yamada, I. Yamada, S. Yamaguchi, M. Yokoyama, R. Akiyama, H. Chikaraishi, K. Haba, S. Hamaguchi, M. Iima, S. Imagawa, N. Inoue, K. Iwamoto, S. Kitagawa, J. Kodaira, Y. Kubota, R. Maekawa, T. Mito, T. Nagasaka, A. Nishimura, C. Takahashi, K. Takahata, Y. Takita, H. Tamura, T. Tsuzuki, S. Yamada, K. Yamauchi, N. Yanagi, H. Yonezu, Y. Hamada, K. Matsuoka, K. Murai, K. Ohkubo, I. Ohtake, M. Okamoto, S. Satoh, T. Satow, S. Sudo, S. Tanahashi, K. Yamazaki, M. Fujiwara, and O. Motojima, "Overview of the Large Helical Device project," Nucl. Fusion **39**, 1245 (1999).

[2]M. Isobe, K. Ogawa, H. Miyake, H. Hayashi, T. Kobuchi, Y. Nakano, K. Watanabe, A. Uritani, T. Misawa, T. Nishitani, M. Tomitaka, T. Kumagai, Y. Mashiyama, D. Ito, S. Kono, M. Yamauchi, and Y. Takeiri, "Wide dynamic range neutron flux monitor having fast time response for the Large Helical Device," Rev. Sci. Instrum. **85**, 11E114 (2014).

[3]M. Isobe, H. Yamanishi, M. Osakabe, H. Miyake, H. Tomita, K. Watanabe, H. Iwai, Y. Nomura, N. Nishio, K. Ishii, J. H. Kaneko, J. Kawarabayashi, E. Takada, A. Uritani, M. Sasao, T. Iguchi, Y. Takeiri, and H. Yamada, "Fusion product diagnostics planned for large helical device deuterium experiment," Rev. Sci. Instrum. **81**, 10D310 (2010).

[4]L. C. Johnson, C. W. Barnes, H. H. Duong, W. W. Heidbrink, D. L. Jassby, M. J. Loughlin, A. L. Roquemore, E. Ruskov, and J. D. Strachan, "Cross calibration of neutron detectors for deuterium-tritium operation in TFTR," Rev. Sci. Instrum. **66**, 894 (1995).

[5]C. W. Barnes, E. B. Nieschmidt, A. G. A. Huibers, L. P. Ku, R. W. Motley, and T. Saito, "Operation and cross calibration of the activation foil system on TFTR," Rev. Sci. Instrum. **61**, 3190 (1990).

[6]C. W. Barnes, H.-S. Bosch, H. W. Hendel, A. G. A. Huibers, D. L. Jassby, R. W. Motley, E. B. Nieschmidt, T. Saito, J. D. Strachan, M. Bitter, R. V. Budny, K. W. Hill, D. K. Mansfield, D. C. Mccune, R. Nazikian, H. K. Park, A. T. Ramsey, S. D. Scott, G. Taylor, and M. C. Zarnstorff, "Triton burnup measurements and calculations on TFTR," Nucl. Fusion **38**, 597 (1998).

[7]J. Källne, P. Batistoni, G. Gorini, G. B. Huxtable, M. Pillon, S. Podda, and M. Rapisarda, "Triton burnup measurements in JET using a neutron activation technique," Nucl. Fusion **28**, 1291 (1988).

[8]M. Hoek, H.-S. Bosch, and W. Ullrich, "Triton burnup measurements at ASDEX upgrade by neutron foil activation," IPP-Report IPP-1/320, 1999.

[9]M. Hoek, T. Nishitani, M. Carlsson, and T. Carlsson, "Triton burnup measurements by neutron activation at JT-60U," Nucl. Instrum. Methods Phys. Res., Sect. A **368**, 804 (1996).

[10] MCNP6 Users Muanual, LA-CP-13–00634, edited by D. Pelowits, Los Alamos National Laboratory, 2013.

[11]E. B. Nieschmidt, T. Saito, C. W. Barnes, H.-S. Bosch, and T. J. Murphy, "Calibration of the TFTR neutron activation system," Rev. Sci. Instrum. **59**, 1715 (1988).

[12]D. B. Syme, S. Popovichev, S. Conroy, I. Lengar, L. Snoj, C. Sowden, L. Giacomellid, G. Hermona, P. Allan, P. Macheta, D. Plummer, J. Stephens, P. Batistoni, R. Prokopowicz, S. Jednorog, M. R. Abhangi, R. Makwanag, and JET EFDA Contributors, "Fusion yield measurements on JET and their calibration," Fusion Eng. Des. **89**, 2766 (2014).

[13]M. Angelone, P. Batistoni, L. Bertalot, B. Esposito, M. Martone, M. Pillon, S. Podda, M. Rapisarda, and S. Roliet, "Experimental and numerical calibration of the neutron activation system on the FTU tokamak," Rev. Sci. Instrum. **61**, 3157 (1990).

[14]T. Sato, K. Niita, N. Matsuda, S. Hashimoto, Y. Iwamoto, S. Noda, T. Ogawa, H. Iwase, H. Nakashima, T. Fukahori, K. Okumura, T. Kai, S. Chiba, T. Furuta, and L. Sihver, "Particle and heavy ion transport code system, PHITS, version 2.52," J. Nucl. Sci. Technol. **50**, 913 (2013).

[15]M. Hoek, T. Nishitani, Y. Ikeda, and A. Morioka, "Initial results from neutron yield measurements by activation technique at JT-60U," JAERI-M 94–002, Japan Atomic Energy Research Institute, 1994.

[16]R. A. Forrest, C. Kalbach Walker, M. Avrigeanu, V. Avrigeanu, F. Tárkányi, A. Trkov, J. Kopecky, and U. Fischer, "FENDL-3 Library - Final Report of the Coordinated Research Project on Nuclear Data Libraries for Advanced Systems: Fusion Devices," IAEA Report INDC(NDS)-0645, IAEA, Vienna, Austria, December 2013.

[17]K. Kobayashi, T. Iguchi, S. Iwasaki, T. Aoyama, S. Shimakawa, Y. Ikeda, N. Odano, K. Sakurai, K. Shibata, T. Nakagawa, and M. Nakazawa, "JENDL dosimetry file 99 (JENDL/D-99)," JAERI 1344, Japan Atomic Energy Research Institute, January 2002.